Supplemental Data. Petsch et al. (2015). Plant Cell 10.1105/tpc.15.00194

Novel DICER-LIKE1 siRNAs Bypass the Requirement for DICER-LIKE4 in Maize Development

Katherine Petsch[1], Priscilla S. Manzotti[2], Oliver H. Tam[1], Robert Meeley[3], Molly Hammell[1], Gabriella Consonni[2], and Marja C. P. Timmermans[1,4]

[1] Cold Spring Harbor Laboratory, One Bungtown Road, Cold Spring Harbor, NY 11724, USA
[2] Dipartimento di Scienze Agrarie e Ambientali, Università degli Studi di Milano, Via Celoria 2, 20133 Milano, Italia
[3] DuPont Pioneer Ag Biotech Research, Johnston, IA 50131, USA

[4]Current address: ZMBP - Developmental Genetics and Cell Biology
University of Tübingen
Auf der Morgenstelle 32
72076 Tübingen
Germany

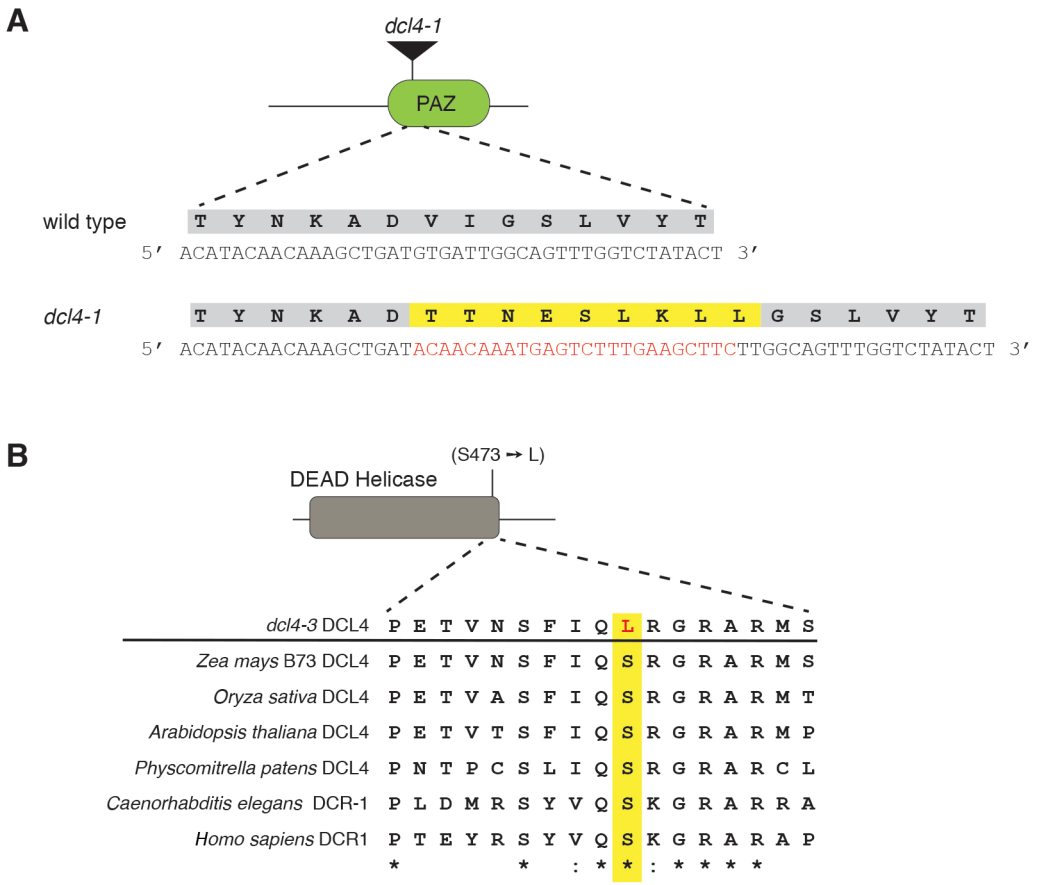

Supplemental Figure 1. Amino acid substitutions in mutant alleles of *dcl4*. (A) The *dcl4-1* allele contains a small rearrangement in the PAZ domain, resulting in a net gain of 21-nt. This alteration translates into nine amino acids that deviate from the wild type sequence but does not affect the downstream reading frame. (B) The *dcl4-3* allele harbors a point mutation in the conserved Helicase C domain, resulting in a nonsynonymous substitution from serine to leucine at position 473.

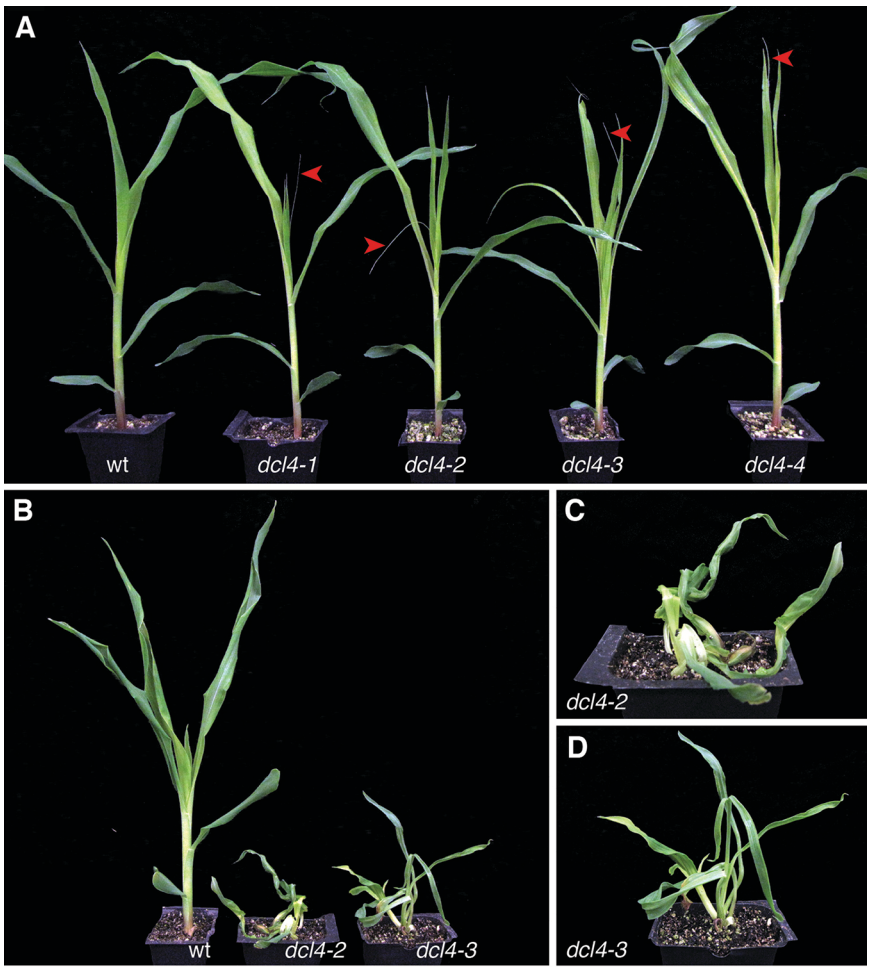

Supplemental Figure 2. The different *dcl4* alleles condition a comparably mild phenotype. (A) Introgression of all four *dcl4* alleles into the B73 inbred line yields plants that exhibit a comparably mild leaf phenotype associated with a variable loss of adaxial identity. The arrows mark the occasional radial, thread-like leaves that are produced. (B-D) The phenotypes of *dcl4-2* and *dcl4*-3 are similarly enhanced upon introgression into the A619 inbred. In this genetic background, growth of the *dcl4* mutants is distorted, internodes fail to elongate, and mutant leaves display a reduced expansion along the mediolateral axis.

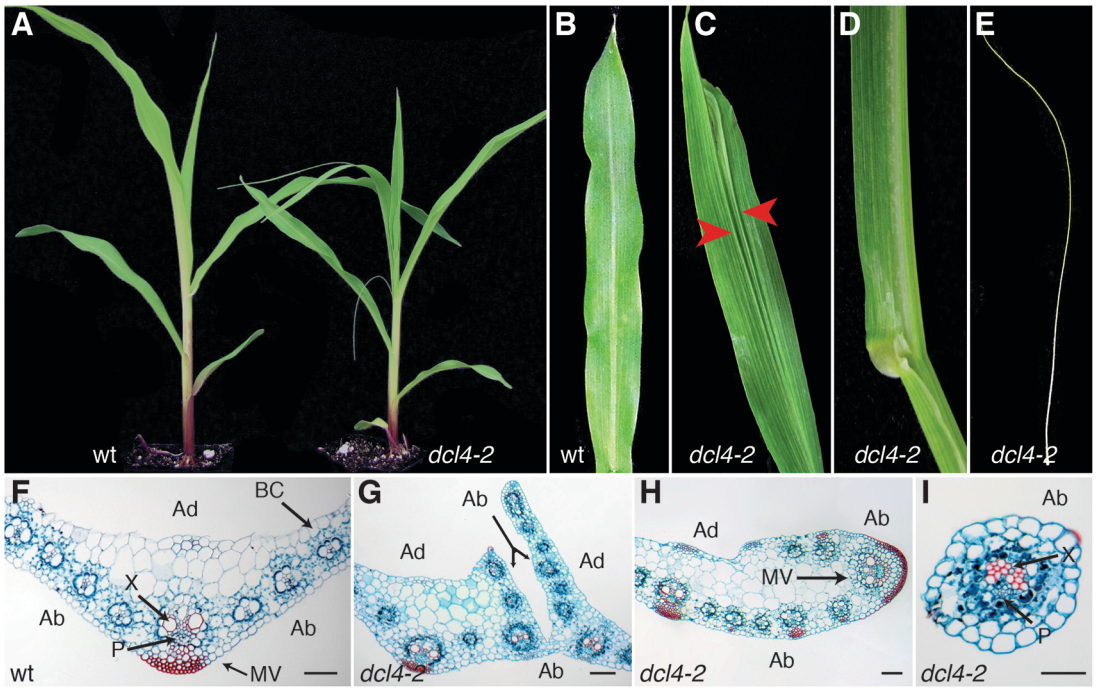

Supplemental Figure 3. *dcl4* mutants exhibit defects in adaxial-abaxial leaf polarity. (A-E) Compared to wild type (A, B), *dcl4* seedlings (A) show a range of leaf expansion defects associated with a variable loss of adaxial-abaxial polarity. *dcl4* leaves often develop ectopic blade outgrowths (arrows) on the upper surface that can occur concomitantly with a bifurcation of the leaf tip (C). Additionally, *dcl4* leaves can show a loss of blade expansion and develop as half (D) or radial, thread-like leaves (E). Leaf-like organs in the inflorescences are affected similarly, and while *dcl4* plants may produce fertile ears, mutants are male sterile. (F) In the wild type leaf, clear cells and sclerenchyma differentiate adaxial and abaxial to the midvein, respectively, and the ligule, macrohairs, and bulliform cells mark the adaxial epidermis. Within the vasculature, xylem differentiates adaxially to phloem. (G) Transverse sections show that ectopic blade outgrowths in *dcl4* occur in pairs around regions of abaxial identity such that vascular bundles are oriented with phloem tissue facing inward. (H) *dcl4* half leaves are associated with a partial loss of adaxial identity resulting in a semi-radial arrangement of vascular bundles around the midvein (right). (I) Thread-like *dcl4* leaves exhibit a radial symmetry with concentric rings of bundle sheath, mesophyll, and epidermal cells surrounding a central vasculature. Such leaves show loss of adaxial characters from the epidermis and ground tissue, but a near normal polarization of the central vasculature. Ad, adaxial; Ab, abaxial; BC, bulliform cell; X, xylem; P, phloem; MV, midvein. Scale bars = 100 μm. (Note panel A has been duplicated from Figure 1B).

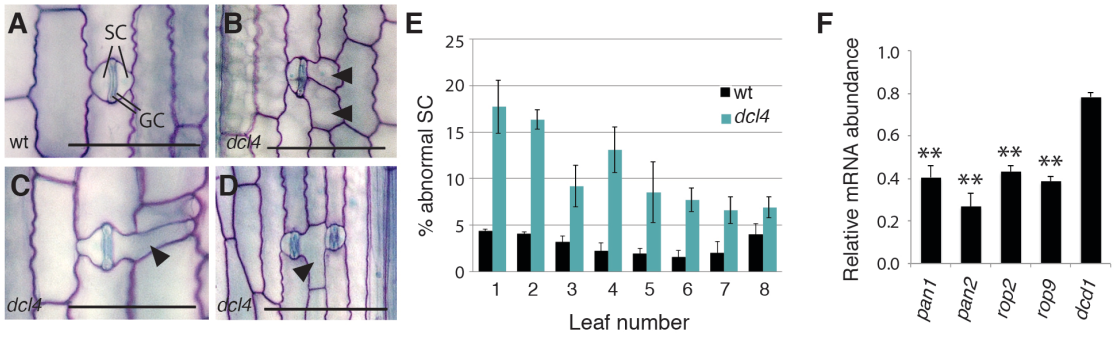

Supplemental Figure 4. *dcl4* affects the asymmetric divisions of subsidiary cells within the stomatal complex. Introgression of *dcl4* alleles into the A619 inbred background enhances their phenotype, although these remain less severe than other ta-siRNA pathway mutants. (A) In A619, *dcl4* mutants display a stomatal defect that had not immediately been noted in B73. The maize stomatal complex consists of two guard cells (GC) each flanked by a single subsidiary cell (SC). The latter arise in response to a signal from the guard mother cell that polarizes the neighboring cells (referred to as subsidiary mother cells) and triggers their asymmetric division to yield the small subsidiary cell and a larger pavement cell (Facette and Smith, 2012). The guard mother cell subsequently undergoes a symmetric cell division to form the two guard cells. (B-D) *dcl4* affects the asymmetric division of subsidiary mother cells resulting in stomatal complexes with abnormally shaped subsidiary cells (arrows). (E) The frequency of abnormally shaped subsidiary cells is increased in *dcl4* versus wild type leaves, particularly in the first juvenile leaves. (F) The defects in subsidiary mother cell division seen in *dcl4* closely resemble those of plants defective for the LRR-receptor-like kinases PANGLOSS1 (PAN1) and PAN2. Both PAN1 and PAN2 form part of the signaling pathway that acts to polarize the subsidiary mother cells prior to asymmetric cell division (Cartwright et al. 2009; Zhang et al. 2012). qRT-PCR analysis shows that transcript levels for both PAN proteins, as well as two ROP GTPases (ROP2 and ROP9) that have been shown to interact physically with PAN1 (Humphries et al. 2011), are significantly reduced in juvenile leaf tissue from *dcl4*, whereas expression of *discordia1* (*dcd1*), which affects cytokinesis more generally (Gallagher et al. 1999), is unchanged. Expression values (means ±SE) normalized to wild type were calculated based on at least three independent biological replicates (**$p < 0.01$). SC, subsidiary cell; GC, guard cell. Scale bars = 100 μm.

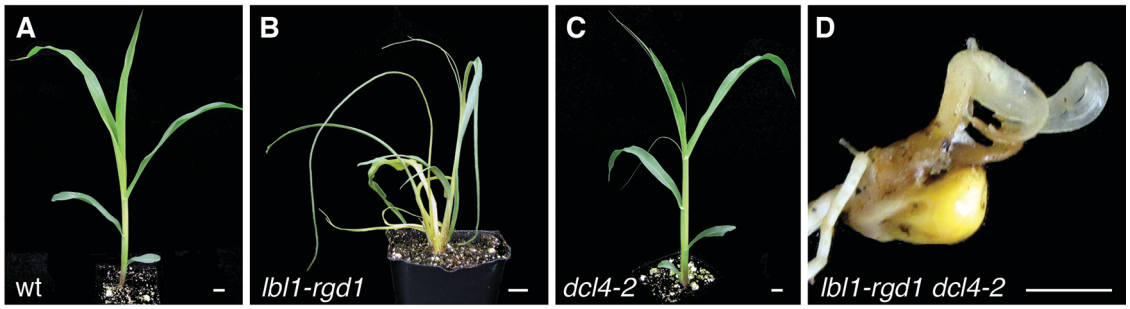

Supplemental Figure 5. *lbl1-rgd1* retains partial tasiR-ARF activity. (A-C) Compared to wild type (A), *lbl1-rgd1* mutants (B) exhibit a severe leaf polarity phenotype, whereas the polarity defects conditioned by the *dcl4-2* null allele (C) are notably milder. (D) Double mutants between *lbl1-rgd1* and *dcl4-2* show a dramatically enhanced phenotype, and frequently arrest shoot development shortly after germination. The *lbl1-rgd1 dcl4-2* phenotype closely resembles the defects resulting from loss of RGD2 or RDR6 activity. Considering that *dcl4-2* is a null allele, this genetic interaction suggests that *lbl1-rgd1* retains partial function. Scale bars = 1cm.

dicer-like1

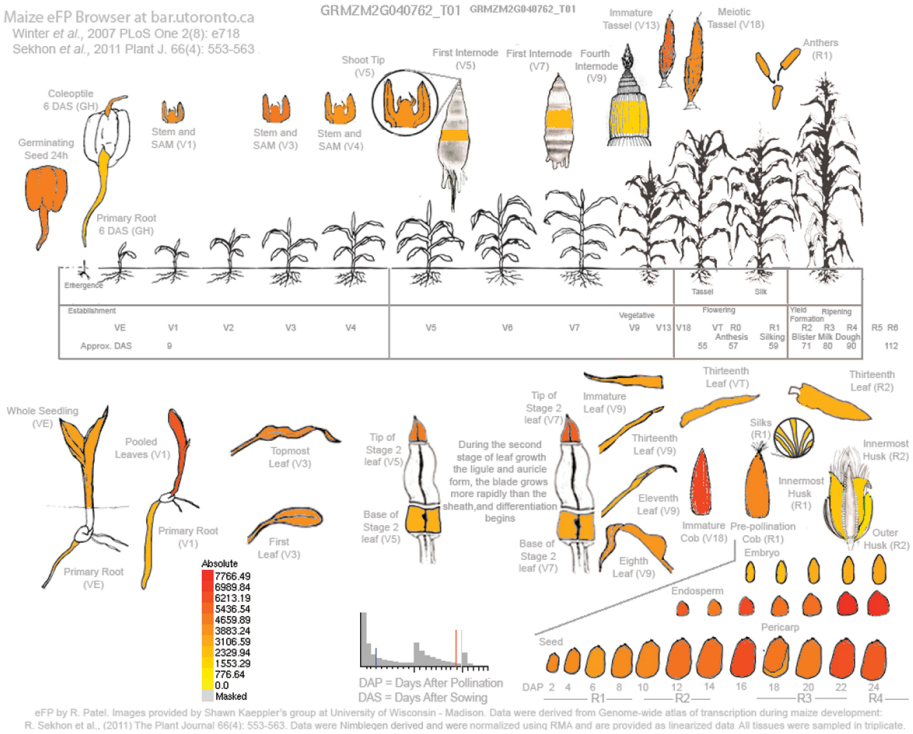

dicer-like2

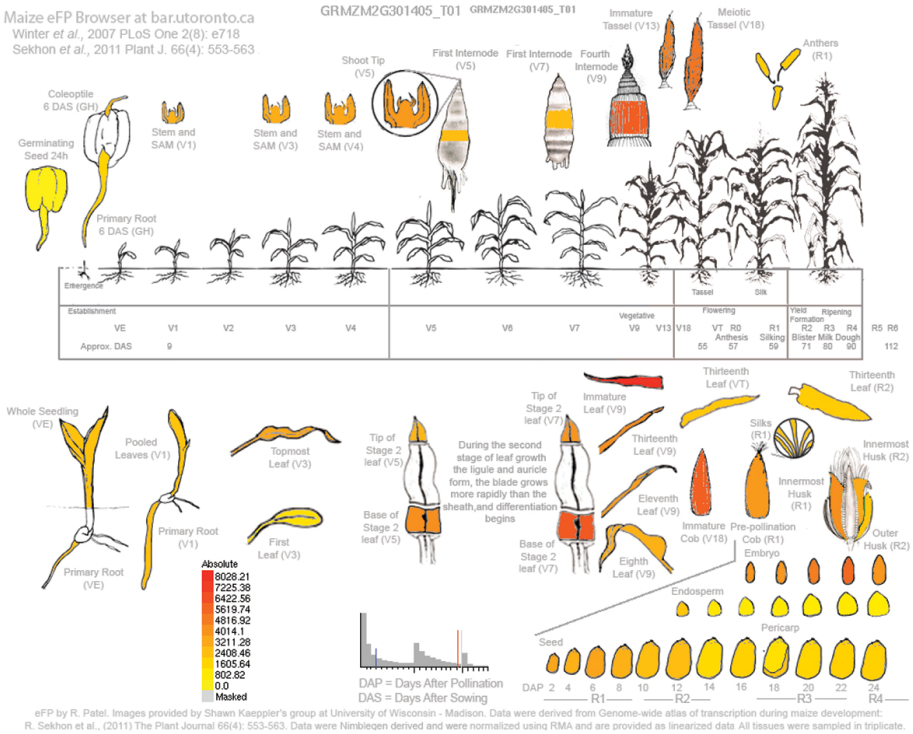

dicer-like3a

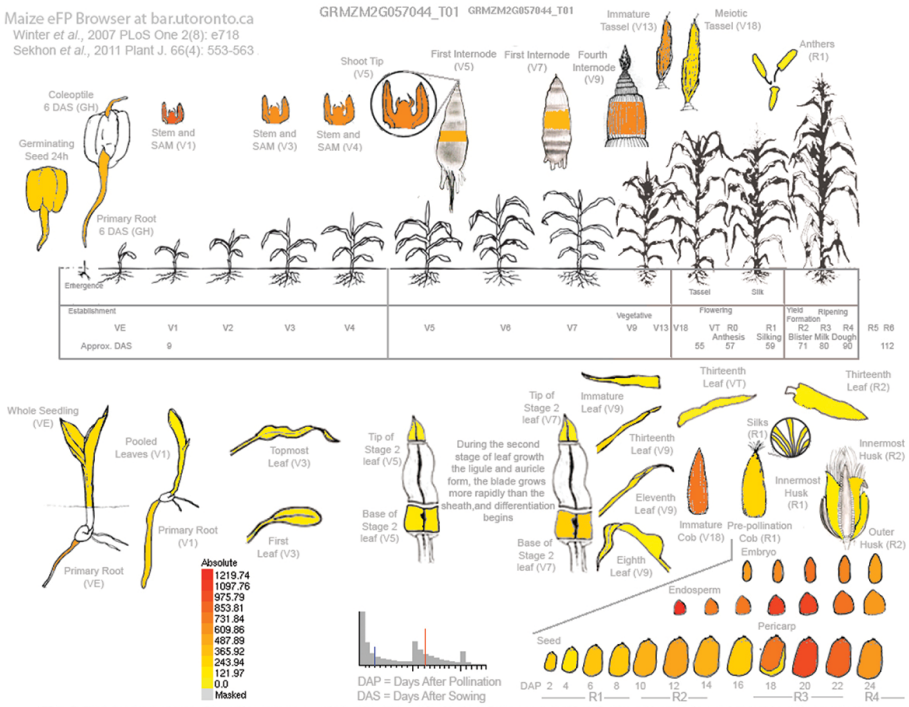

eFP by R. Patel. Images provided by Shawn Kaeppler's group at University of Wisconsin - Madison. Data were derived from Genome-wide atlas of transcription during maize development: R. Sekhon et al., (2011) The Plant Journal 66(4): 553-563. Data were Nimblegen derived and were normalized using RMA and are provided as linearized data. All tissues were sampled in triplicate.

dicer-like3b /dicer-like5

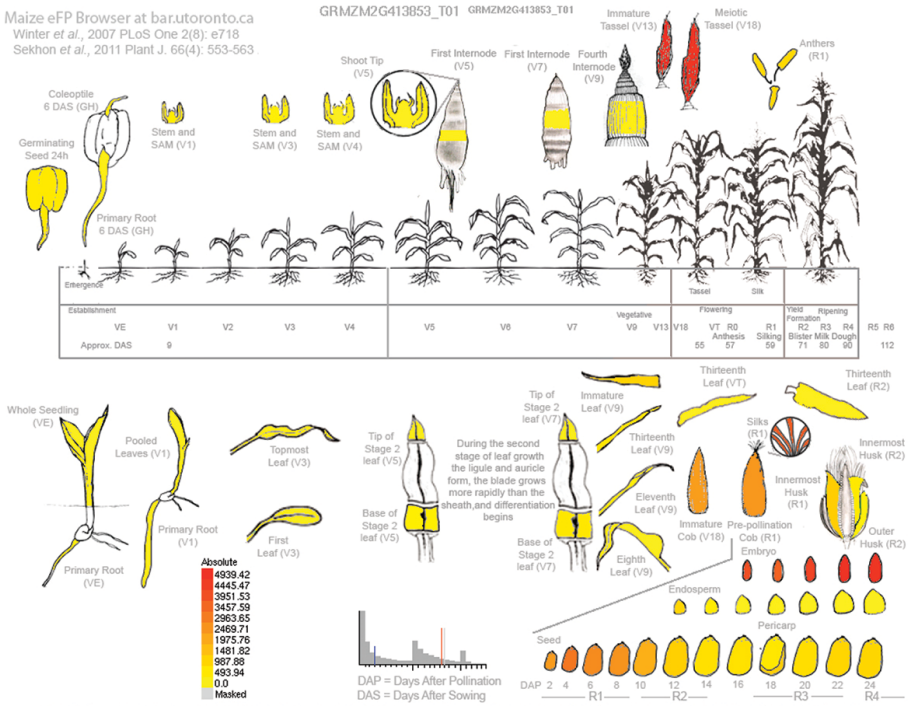

eFP by R. Patel. Images provided by Shawn Kaeppler's group at University of Wisconsin - Madison. Data were derived from Genome-wide atlas of transcription during maize development: R. Sekhon et al., (2011) The Plant Journal 66(4): 553-563. Data were Nimblegen derived and were normalized using RMA and are provided as linearized data. All tissues were sampled in triplicate.

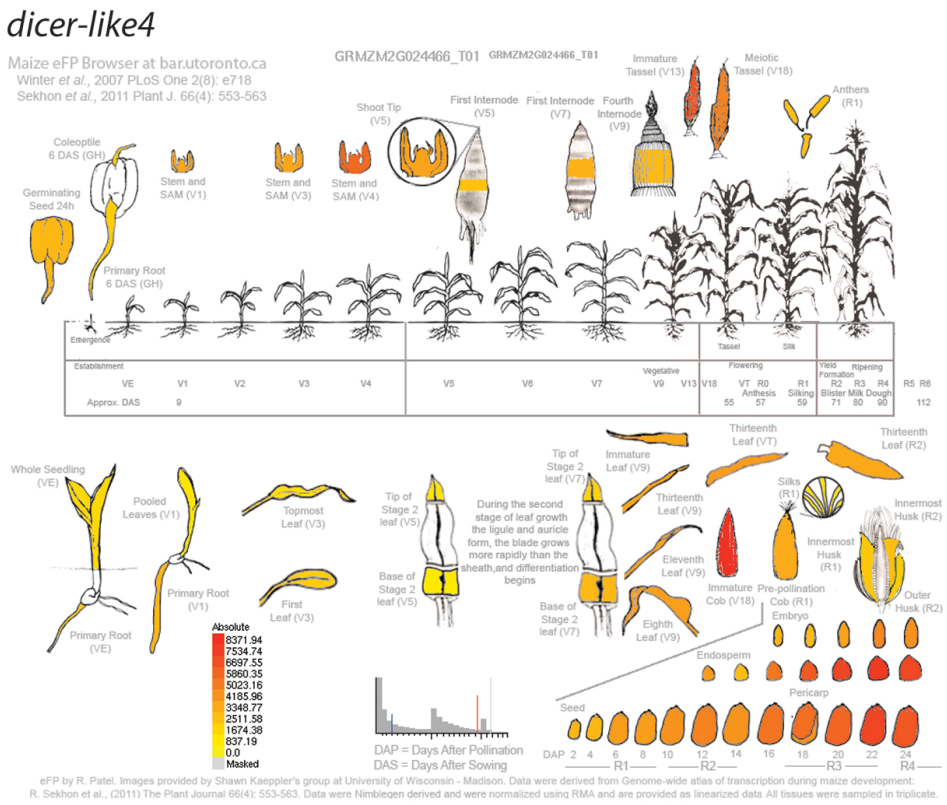

Supplemental Figure 6. Global expression profiles of the five maize *dicer-like* genes show that while *dcl1, dcl2, dcl3a,* and *dcl4* are expressed broadly throughout plant development, *dcl3b/dcl5* is expressed primarily during reproductive development and in the immature embryo. eFP browser images based on data from Sekhon et al. (2011) are shown.

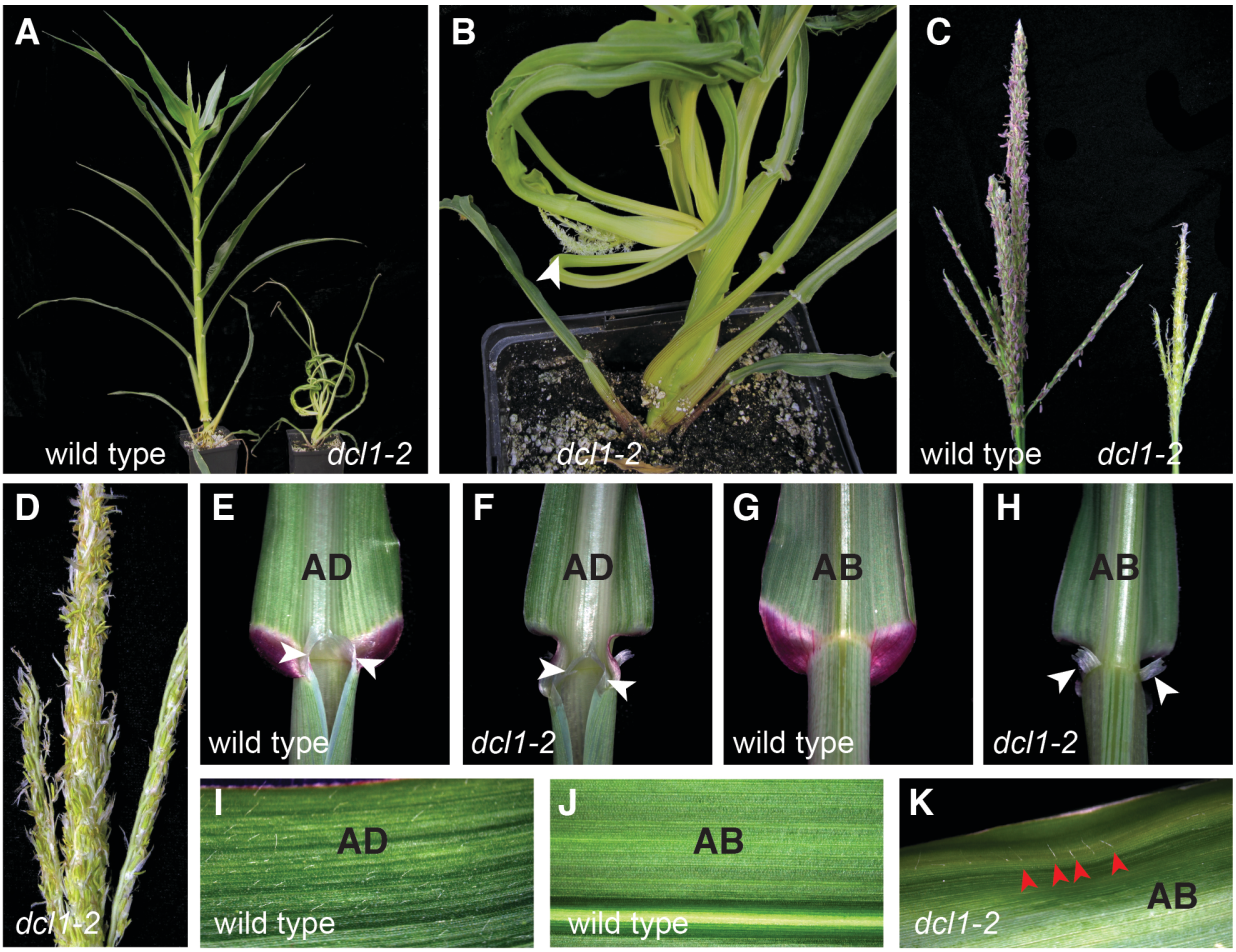

Supplemental Figure 7. *dcl1-2* conditions a weakly adaxialized leaf polarity phenotype. (A) Compared to wild type, *dcl1-2* mutants are severely stunted and develop narrow upward curled leaves. (B-D) Inflorescence development typically arrests at an early stage, and *dcl1-2* mutants are both male and female sterile. Arrow in (B) indicates a malformed tassel. Occasionally, mildly phenotypic mutants develop a more normal tassel morphology, but any anthers produced lack viable pollen (C, D). (E-K) *dcl1-2* leaves are weakly adaxialized. In wild type, the ligule forms at the sheath-blade junction on the adaxial side of the leaf (E, G). In addition to the normal ligular fringe (F), *dcl1-2* leaves develop ectopic ligules on the abaxial side of the leaf (arrows in H). Similarly, macrohairs that distinguish the adaxial blade epidermis in wild type (I, J) are present in sectors on the abaxial blade surface of *dcl1-2* leaves (arrows in K).

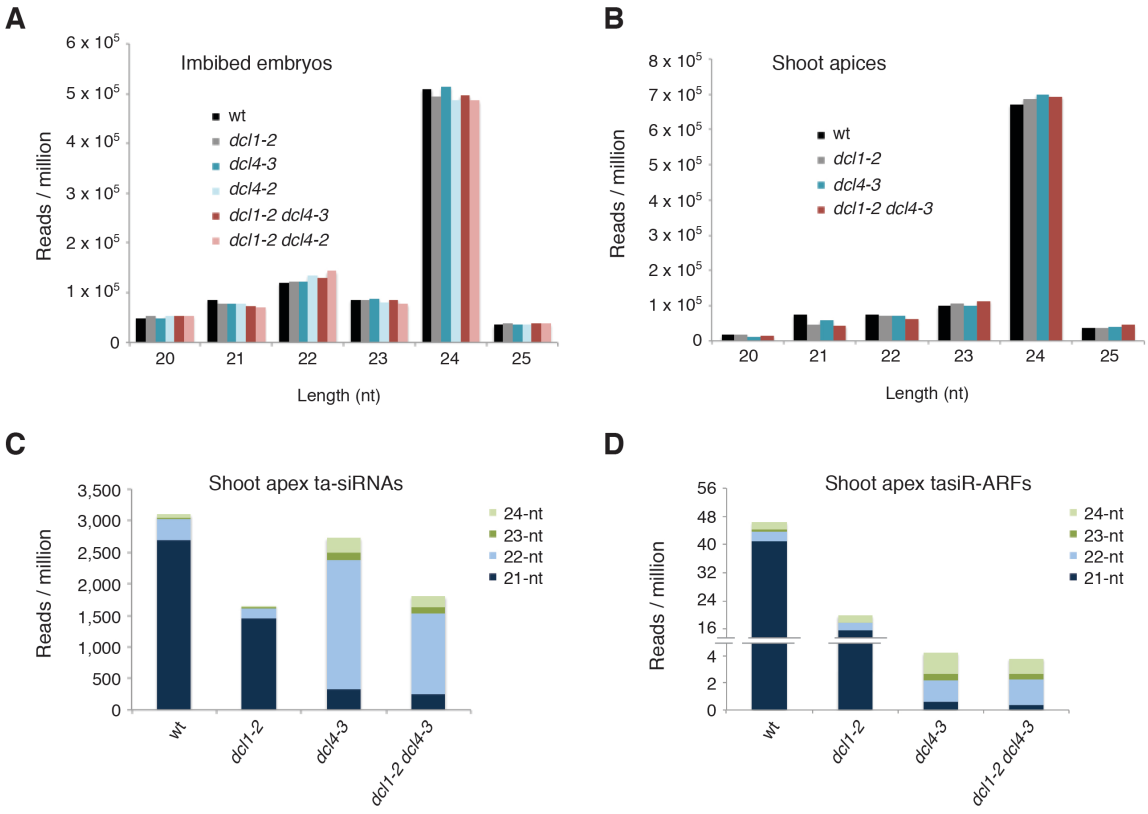

Supplemental Figure 8. *dcl1* and *dcl4* mutants show defined changes in small RNA content. (A, B) Size distribution profiles of small RNAs in libraries from imbibed embryos (A) and shoot apices (B) show that the overall small RNA populations are minimally changed between genotypes. (C) In *dcl4-3* single and *dcl1-2 dcl4-3* double mutants, ta-siRNAs derived from the nine *TAS3* loci show a shift in size and are predominantly 22- rather than 21-nt in length. (D) The tasiR-ARFs also deviate from their normal 21-nt size but show little change in accumulation between *dcl4-3* and the *dcl1-2 dcl4-3* double mutant.

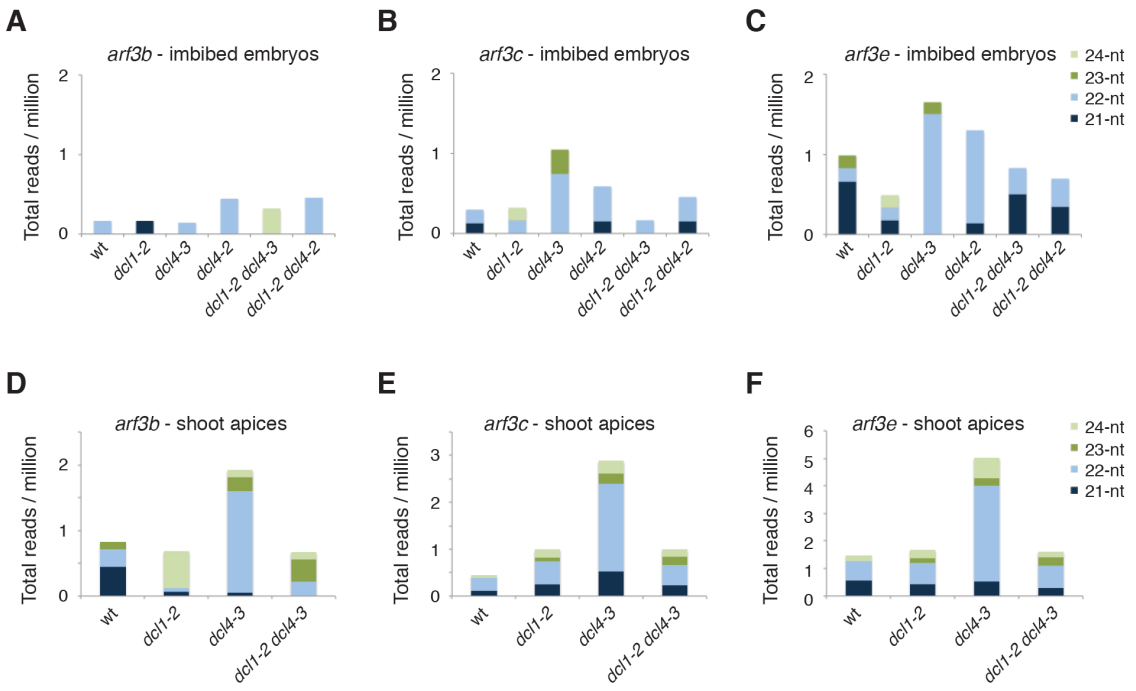

Supplemental Figure 9. *arf3b-, c-* and *e*-derived small RNAs are present at low levels in *dcl4* imbibed embryos and shoot apices. (A-F) Low levels of *arf3b-, c-*, and *e*-derived siRNAs accumulate in imbibed embryos (A-C) and shoot apices (D-F) of wild type, *dcl1-2, dcl4-2, dcl4-3*, and their respective double mutants. For comparison, *arf3d*-derived siRNAs accumulate to approximately 100- and 400-fold higher levels in imbibed embryos and vegetative apices of *dcl4* mutants, respectively.

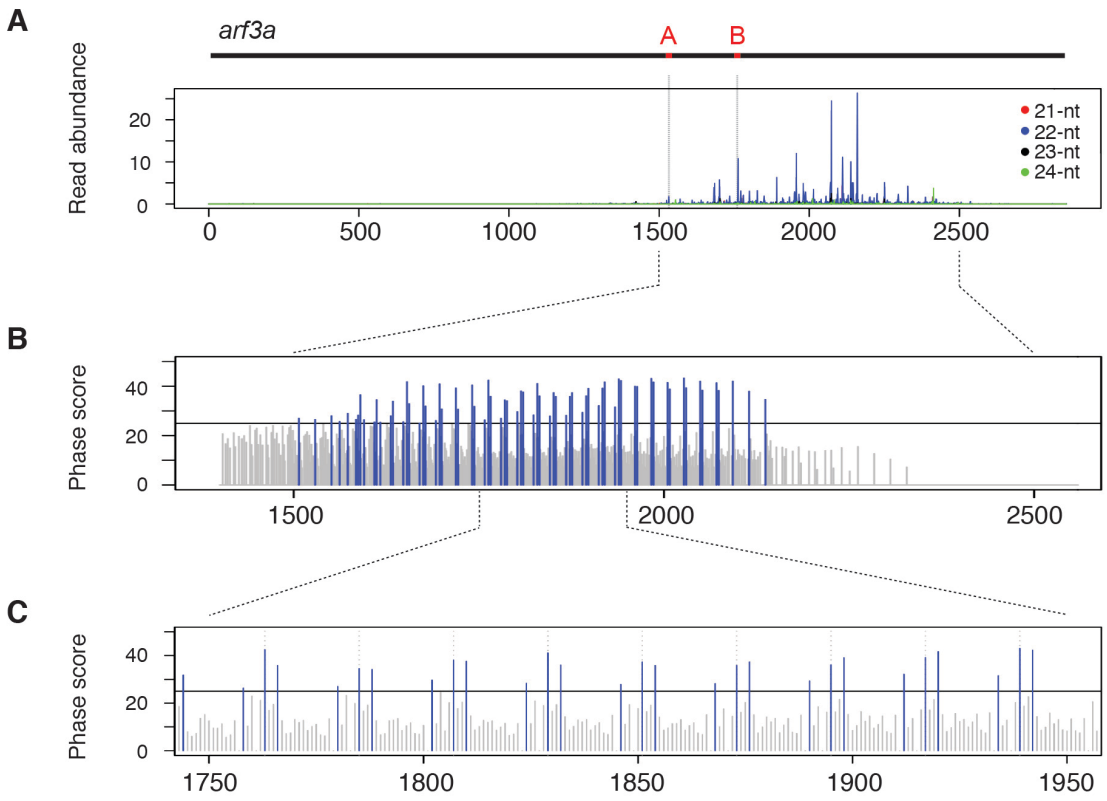

Supplemental Figure 10. In *dcl4* mutants, *arf3a* transcripts are processed into 22-nt phased siRNAs. (A) The *arf3a*-derived DCL1-dependent siRNAs generated in *dcl4* mutants are abundant, mostly 22-nt in length, and originate from transcribed regions downstream of the two tasiR-ARF target sites (A and B). These are indicated in red on the *arf3a* transcript, and vertical grey lines mark their position relative to siRNA accumulation. (B, C) The 22-nt *arf3a*-derived siRNAs are phased, although in contrast to the simple phasing register observed for miRNA triggered secondary siRNAs, the phasing pattern for the *arf3a*–derived siRNAs is more complex. Considering a one-hit mechanism of biogenesis, the two tasiR-ARF target sites are predicted to generate distinct but overlapping 22-nt phasing registers. Moreover, in *dcl4* mutants, the hierarchical activity of other DCL enzymes also leads to the production of 22-nt tasiR-ARF variants that are offset by 1-2 nt, which along with feedback from the 22-nt *arf3a*-derived secondary siRNAs further confound the phasing pattern. Blue lines, siRNA registers with a Phasing score >25; Grey lines, siRNA registers with a Phasing score <25; Dashed grey lines, 22-nt windows.

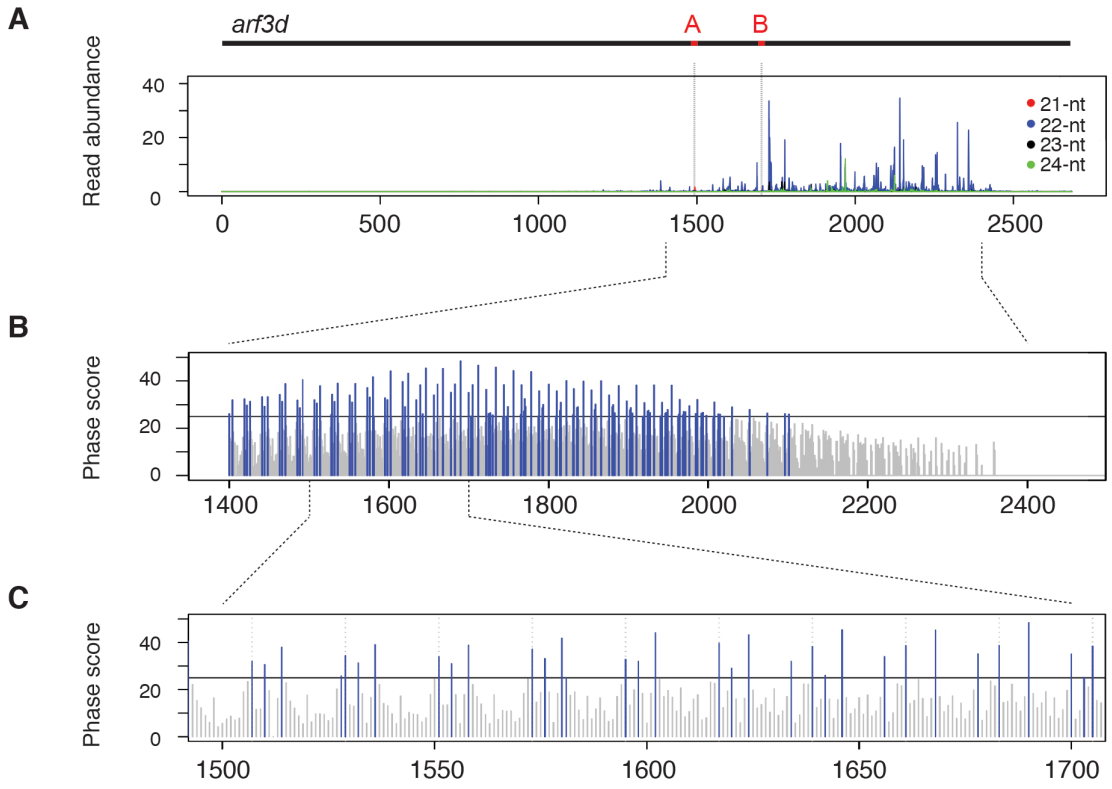

Supplemental Figure 11. *arf3d* transcripts are similarly processed into 22-nt phased siRNAs in *dcl4* mutants. (A) Analogous to *arf3a*, the *arf3d*-derived DCL1-dependent siRNAs generated in *dcl4* mutants are abundant, mostly 22-nt in length, and originate from transcribed regions downstream of the two tasiR-ARF target sites (A and B). These are indicated in red on the *arf3d* transcript, and vertical grey lines mark their position relative to siRNA accumulation. (B, C) The 22-nt *arf3d*-derived siRNAs are phased and also exhibit a complex phasing pattern. Blue lines, siRNA registers with a Phasing score >25; Grey lines, siRNA registers with a Phasing score <25; Dashed grey lines, 22-nt windows.

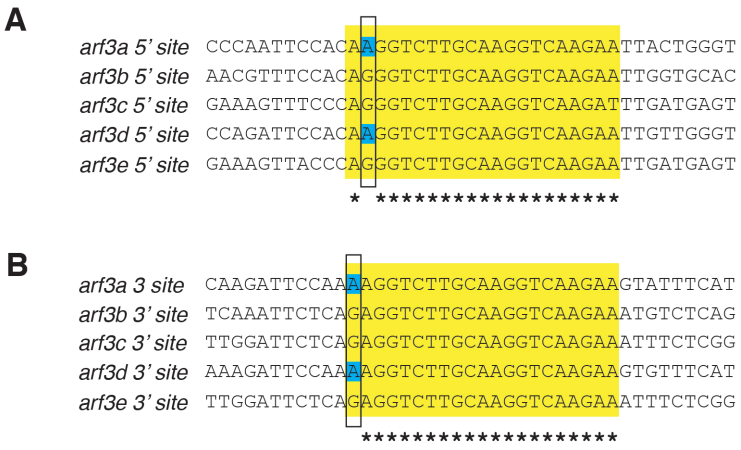

Supplemental Figure 12. SNPs in the tasiR-ARF recognition sites distinguish *arf3a* and *arf3d* from the remaining *arf3* genes. (A, B) The *arf3* target transcripts each contain two tasiR-ARF target sites (highlighted in yellow). The 5' most target sites (A) are identical in sequence except at position 2, which is an 'A' in *arf3a* and *arf3d*, and a 'G' in *arf3b, c* and *e*. The 3' most target sites (B) likewise contain a single polymorphism, although at position 1. This SNP is an 'A' in *arf3a* and *arf3d*, and a 'G' in the other *arf3* members. Boxes in (A) and (B) indicate the position of the SNPs. The presence of an asterisk below the tasiR-ARF recognition sites denotes 100% nucleotide identity.

Supplemental Table 1. Summary analysis for small RNA libraries.

Tissue	Genotype	18-26 nt reads	Genome-matched reads	% Mapped	Reads mapped < 20	% Mapped < 20
Imbibed embryo	wt (rep1)	11,302,552	8,635,396	76.4	3,854,255	34.1
	wt (rep2)	8,811,010	6,610,856	75.0	3,032,961	34.4
	dcl1-2 (rep1)	9,100,660	6,985,978	76.8	2,902,390	31.9
	dcl1-2 (rep2)	9,415,542	7,148,735	75.9	3,130,486	33.2
	dcl4-3 (rep1)	10,546,900	8,072,698	76.5	3,439,148	32.6
	dcl4-3 (rep2)	9,238,501	6,959,708	75.3	3,193,819	34.6
	dcl4-2 (rep1)	10,050,589	7,673,106	76.3	3,491,795	34.7
	dcl4-2 (rep2)	10,089,639	7,679,107	76.1	3,352,304	33.2
	dcl1-2 dcl4-3 (rep1)	9,595,561	7,343,182	76.5	3,166,222	33.0
	dcl1-2 dcl4-3 (rep2)	9,642,119	7,673,562	79.6	2,928,044	30.4
	dcl1-2 dcl4-2 (rep1)	7,721,695	5,824,050	75.4	2,542,864	32.9
	dcl1-2 dcl4-2 (rep2)	9,834,892	7,722,735	78.5	3,262,289	33.2
Shoot apices	wt	34,970,126	31,064,237	88.8	18,137,287	51.9
	dcl1-2	33,086,705	28,970,602	87.6	15,992,213	48.3
	dcl4-3	33,792,682	30,078,300	89.0	18,750,442	55.5
	dcl1-2 dcl4-3	38,144,109	33,993,889	89.1	17,937,929	47.0

Supplemental Table 2. miRNA abundance (RPM) in imbibed embryos.

miRNA Family	wt (rep1)	wt (rep2)	*dcl1-2* (rep1)	*dcl1-2* (rep2)	*dcl4-3* (rep1)	*dcl4-3* (rep2)	*dcl4-2* (rep1)	*dcl4-2* (rep2)	*dcl1-2 dcl4-3* (rep1)	*dcl1-2 dcl4-3* (rep2)	*dcl1-2 dcl4-2* (rep1)	*dcl1-2 dcl4-2* (rep2)
miR156	1136.1	1210.0	730.9	790.9	1175.7	1115.1	1157.0	1213.2	911.0	685.0	572.0	622.9
miR159	1478.8	1929.9	966.7	935.0	1419.0	1468.2	1369.8	1328.7	828.2	813.9	680.1	879.6
miR160	26.2	36.8	8.0	10.7	24.7	22.0	18.3	22.5	9.1	8.5	21.1	11.2
miR162	23.1	17.8	3.1	7.0	18.9	11.3	16.6	19.7	7.0	8.2	9.4	5.8
miR164	99.3	117.8	49.1	72.9	149.1	131.0	129.4	91.3	100.1	79.0	106.9	150.7
miR166	4956.9	5975.0	2207.3	2528.1	4996.1	4646.2	4303.3	3357.0	2435.8	2226.2	1616.6	1315.1
miR167	371.9	393.1	277.8	324.5	374.2	360.3	369.2	283.5	319.7	316.4	349.8	288.8
miR168	71.9	89.4	25.8	18.9	82.6	91.4	84.2	112.8	19.9	18.4	26.0	15.3
miR169	48.5	70.7	14.6	12.3	50.5	44.9	75.3	84.0	13.5	14.0	23.7	17.5
miR171	45.0	85.7	15.1	30.4	37.9	51.8	38.8	50.3	27.2	15.0	18.4	9.6
miR172	0.00	1.7	0.7	0.3	0.3	0.9	0.3	0.9	0.3	0.3	0.4	0.0
miR319	3148.7	3890.9	1320.3	1265.0	3236.9	2828.9	3656.6	3585.3	1112.7	1038.9	1250.6	1085.7
miR390	8.1	8.9	3.9	5.2	11.2	13.7	7.2	10.1	3.5	6.2	3.0	4.3
miR393	22.3	28.0	16.9	13.1	19.2	25.5	19.6	15.2	12.2	11.8	7.9	9.5
miR394	13.1	14.2	0.0	0.5	11.2	20.51	6.5	10.4	8.8	13.7	4.7	6.6
miR395	7.1	4.3	3.4	4.5	4.2	4.95	4.0	5.4	4.7	3.0	3.1	3.7
miR396	308.1	373.6	123.1	160.5	271.4	337.1	354.5	304.6	126.5	147.5	174.8	180.6
miR397	48.5	62.7	21.7	41.2	39.3	50.72	158.7	74.9	29.7	26.0	64.9	69.6
miR398	76.5	88.7	15.2	16.6	64.0	67.00	191.9	230.3	12.0	12.0	79.4	47.5
miR399	0.3	0.3	0.4	0.0	0.3	0.00	0.3	0.0	0.0	0.0	0.0	0.0
miR408	300.5	251.2	143.7	208.9	198.9	211.35	647.2	281.0	211.9	157.8	502.6	316.0
miR528	129.5	119.4	30.7	49.8	84.9	72.64	326.8	183.2	35.1	27.0	144.7	134.6
miR529	9.9	10.2	2.8	3.5	11.9	10.96	9.7	11.0	5.1	2.4	3.2	3.7
miR827	364.3	432.9	249.1	236.1	405.3	457.45	618.3	527.7	270.7	276.0	46.0	72.3
miR1432	0.3	1.0	0.0	0.0	0.9	0.63	0.0	0.6	0.6	0.7	0.0	0.0
miR2118	2.2	3.0	0.3	0.3	2.2	0.94	3.4	3.0	0.6	0.3	1.2	0.0
miR2275	2.0	0.3	0.9	1.7	3.2	0.31	1.4	0.6	0.5	0.5	0.4	2.2

Supplemental Table 3. Two-tailed t-test comparisons for miRNA levels in imbibed embryos of various *dcl* mutants.

Comparison	p-value		
	Total miRNAs	miR390a	miR390b
wt vs. *dcl1-2*	0.0282	0.0103	0.0620
wt vs. *dcl4-3*	0.3463	0.1030	0.1066
wt vs. *dcl4-2*	0.4953	0.8782	0.9951
wt vs. *dcl1-2 dcl4-3*	0.0267	0.1342	0.1080
wt vs. *dcl1-2 dcl4-2*	0.0220	0.0118	0.0367
dcl4-3 vs. *dcl1-2 dcl4-3*	0.0050	0.0631	0.0055
dcl4-2 vs. *dcl1-2 dcl4-2*	0.0155	0.0897	0.0936
dcl1-2 vs. *dcl1-2 dcl4-3*	0.55262	0.9350	0.1784
dcl1-2 vs. *dcl1-2 dcl4-2*	0.09899	0.8435	0.6681

Supplemental Table 4. Two-tailed t-test comparisons for 21-nt ta-siRNA and tasiR-ARF levels in imbibed embryos.

Comparison	p-value	
	ta-siRNAs	tasiR-ARFs
wt vs. *dcl1-2*	0.0053	0.5652
wt vs. *dcl4-3*	0.0009	0.0448
wt vs. *dcl4-2*	0.0008	0.0313
wt vs. *dcl1-2 dcl4-3*	0.0009	0.0309
wt vs. *dcl1-2 dcl4-2*	0.0030	0.0418
dcl4-3 vs. *dcl1-2 dcl4-3*	0.0644	0.5358
dcl4-2 vs. *dcl1-2 dcl4-2*	0.9638	0.3008

Supplemental Table 5. Primers used for quantitative RT-PCR.

Gene name	Gramene ID	Forward primer sequence	Reverse primer sequence
pan1	GRMZM5G836190	AAGCTGCTCATCTACGACTACCTC	TATTATCCTTGCTCATTGCTATCG
pan2	GRMZM2G034572	GAGAAGCTCATCTTGTCGGATTAC	GGTCGAAGTGGAGGTAGTTGAG
rop2	GRMZM5G846811	CGATTAGGTAACTCGCTTAGAAGG	GGAAGCATACTTTTCCATTCAAGT
rop9	GRMZM5G803949	ATGGAAAATTATGCTTCCCAATTA	CCACAAAGACACTGAGAACTTGAC
dcd1	GRMZM2G083459	ACTGCATTTGTTCAGATGTACTGC	TATCGGTTACCTCTTCCTCACTCT
arf3a	GRMZM2G030710	CTTCCCCATGTTAATCCAGACTAC	CAGCAGCATTGTCATGAGTTCTAT
arf3b	GRMZM2G441325	AAGCTACTTATGCTGTCTGCTGTG	TCTGGTTCCAACTGAAAAGTGATA
arf3c	GRMZM2G056120	GCACAAAAGTGTTTTTCACATTTC	TGTAAGTTGATCCTTGCTCCAATA
arf3d	GRMZM2G437460	ACTCCTATTCCTGCACCTCATAAC	TTGTGAACTTCCAATAGGGTACAA
arf3e	GRMZM5G874163	ATTTCAATAGTGACAGCACAAAGC	CTTCAGGAACTTAGCGTATGGAAT
gapc	GRMZM2G046804	TTCCTGATCTGAATGGCAAG	CTCGGAAGCAGCCTTAATAG

SUPPLEMENTAL REFERENCES

Cartwright, H.N., Humphries, J.A., and Smith, L.G. (2009). PAN1: a receptor-like protein that promotes polarization of an asymmetric cell division in maize. Science **323**: 649-651.

Facette, M.R., and Smith, L.G. (2012). Division polarity in developing stomata. Curr Opin Plant Biol **15**: 585-592.

Gallagher, K., and Smith, L.G. (1999). *discordia* mutations specifically misorient asymmetric cell divisions during development of the maize leaf epidermis. Development **126**: 4623-4633.

Humphries, J.A., Vejlupkova, Z., Luo, A., Meeley, R.B., Sylvester, A.W., Fowler, J.E., and Smith, L.G. (2011). ROP GTPases act with the receptor-like protein PAN1 to polarize asymmetric cell division in maize. Plant Cell **23**: 2273-2284.

Sekhon, R.S., Lin, H., Childs, K.L., Hansey, C.N., Buell, C.R., de Leon, N., and Kaeppler, S.M. (2011). Genome-wide atlas of transcription during maize development. Plant J **66:** 553-563.

Zhang, X., Facette, M., Humphries, J.A., Shen, Z., Park, Y., Sutimantanapi, D., Sylvester, A.W., Briggs, S.P., and Smith, L.G. (2012). Identification of PAN2 by quantitative proteomics as a leucine-rich repeat-receptor-like kinase acting upstream of PAN1 to polarize cell division in maize. Plant Cell **24**: 4577-4589.